



**Environmental  
Science**  
Nano

**Cellulose Nanocrystal/Silver (CNC/Ag) Thin-film  
Nanocomposite Nanofiltration Membranes with  
Multifunctional Properties**

Journal:	<i>Environmental Science: Nano</i>
Manuscript ID	EN-ART-11-2019-001367.R1
Article Type:	Paper

**SCHOLARONE™**  
Manuscripts

1  
2  
3 Cellulose nanocrystals (CNCs), as an emerging low-cost, hydrophilic, bio-renewable  
4 and environmentally friendly additive, have been widely applied in polymer  
5 nanocomposites, biomedical and personal care products. Nanocomposites based on  
6 CNCs are even more promising as the combination of functional materials can exhibit  
7 multi-functions. In this work, we successfully prepared CNC/Silver (Ag)  
8 nanocomposites and incorporated them into the active layer of thin film composite  
9 nanofiltration membranes. The CNC/Ag nanofiltration membranes exhibited high  
10 water flux, high salt rejections, and excellent anti-fouling, and antibacterial  
11 performance simultaneously. Besides, CNC/Ag membranes can achieve a low Ag  
12 releasing rate and long duration time with a small amount of total Ag loading, which  
13 implies its low potential environmental risks and the potential for practical water  
14 treatment.  
15  
16  
17  
18  
19  
20  
21  
22  
23  
24  
25  
26  
27  
28  
29  
30  
31  
32  
33  
34  
35  
36  
37  
38  
39  
40  
41  
42  
43  
44  
45  
46  
47  
48  
49  
50  
51  
52  
53  
54  
55  
56  
57  
58  
59  
60

1  
2  
3  
4  
5  
6  
7  
8  
9  
10  
11  
12  
13  
14  
15  
16  
17  
18  
19  
20  
21  
22  
23  
24  
25  
26  
27  
28  
29  
30  
31  
32  
33  
34  
35  
36  
37  
38  
39  
40  
41  
42  
43  
44  
45  
46  
47  
48  
49  
50  
51  
52  
53  
54  
55  
56  
57  
58  
59  
60

# **Cellulose Nanocrystal/Silver (CNC/Ag) Thin-film Nanocomposite Nanofiltration Membranes with Multifunctional Properties**

Chunyan Xu, Wensi Chen, Haiping Gao, Xing Xie, Yongsheng Chen\*

*School of Civil & Environmental Engineering, Georgia Institute of Technology, Atlanta, GA  
311 Ferst Dr NW, Atlanta, Georgia 30332-0100, United States*

\*Corresponding author: [yongsheng.chen@ce.gatech.edu](mailto:yongsheng.chen@ce.gatech.edu)

## Abstract

The trade-off between membrane permeability and selectivity, as well as membrane fouling including both physical and bio-fouling, are major challenges that limit the practical application of nanofiltration (NF) membranes. In order to address these issues simultaneously, multifunctional membranes with maximized water permeability/salt selectivity, as well as enhanced antifouling and antibacterial properties are desired. In this work, we prepare a novel multifunctional thin film nanocomposites (TFN) NF membrane by embedding cellulose nanocrystal/silver (CNC/Ag) nanocomposites in the polyamide layer. The CNC/Ag TFN NF membranes exhibit excellent properties by taking the advantage of both CNC, a highly hydrophilic, low-cost, bio-renewable, and environmentally friendly nanomaterial, and Ag nanoparticles, one of the most effective bactericidal materials. With the incorporation of only 0.01 wt% CNC/Ag nanocomposites, a high pure water permeability ( $25.4 \text{ L m}^{-2} \text{ h}^{-1} \text{ bar}^{-1}$ ) and a high rejection rate of  $\text{Na}_2\text{SO}_4$  (99.1 %) of CNC/Ag TFN NF membrane can be achieved, respectively. Besides, the membrane also exhibits exceptional antifouling (flux recovery ratio reaches 92.6 % for humic acid) and antibacterial performance (99.4 % reduction of *Escherichia coli* viability). The  $\text{Ag}^+$  leaching test also demonstrates good stability of Ag nanoparticles in the active thin-film layer of the CNC/Ag NF membranes. These findings have strong positive implications towards the development of next-generation high performance NF membranes for water treatment.

## 1. Introduction

Membrane filtration is an energy-efficient and relatively low-cost technology for water treatment and desalination.<sup>1, 2</sup> Nanofiltration (NF) is a pressure-driven separation process, which has been widely used in seawater pretreatment, heavy metal removal, dye removal, and oil-water separation in recent years.<sup>2-5</sup> Currently, most of the commercially available NF membranes are thin film composite (TFC) membranes consisted of an ultrathin polyamide active layer that acts as a selective barrier, and a porous substrate as a support. However, the trade-off between permeability and selectivity, as well as membrane fouling, including biofouling, caused by salts, colloids, macromolecules, and bacteria, have limited a broader application of TFC NF membranes in practical water treatments.<sup>6, 7</sup> In practice, multifunctional NF membranes with high water flux without sacrificing the salt rejection, as well as excellent antifouling and antibacterial performance are crucial for stable, long-term operations in the water treatment process.<sup>8</sup> Previous researchers have been intensively working on solving the above-mentioned problems by fabricating thin-film nanocomposite (TFN) NF membranes via incorporating functional nanomaterials in the thin film layer. Some studies used hydrophilic nanomaterials ( $\text{TiO}_2$ ,<sup>9</sup>  $\text{SiO}_2$ ,<sup>10</sup> graphene oxide,<sup>11</sup> etc.) to yield a higher water flux and better resistance towards the fouling of model pollutants on the membrane; while the others investigated the effect of antimicrobials (silver,<sup>12</sup> Cu,<sup>13</sup> ZnO,<sup>14</sup> etc.) on membrane antibacterial performance. However, mono-functional nanofillers mentioned above can only enhance one single function for host membranes.<sup>15-19</sup> Besides, some of these nanoparticles (NPs) embedded in membranes are harmful to environment and cytotoxic to human cells according to previous studies.<sup>20-22</sup> Thus, TFN NF membranes adding

1  
2  
3  
4 environmental-friendly and stable nanocomposites with multi-functions are needed for  
5  
6 practical water treatment.  
7  
8

9  
10 Cellulose nanocrystals (CNCs) are environmentally friendly, renewable, mechanically strong,  
11  
12 and low-cost nanomaterials, which can be sourced from a wide variety of renewable biomass,  
13  
14 such as cotton, wood, and straw.<sup>23, 24</sup> CNCs are excellent additives for polymer  
15  
16 nanocomposite, biomedical and personal care products,<sup>23</sup> etc. Moreover, CNCs also possess  
17  
18 high hydrophilicity due to the presence of abundant hydroxyl (-OH) groups on the surface,  
19  
20 thus promoting themselves as excellent additives in the modification of separation  
21  
22 membranes.<sup>24</sup> For instance, Bai et al. reported that the water flux, rejection, mechanical  
23  
24 strength, and antifouling performance of both ultrafiltration (UF) and NF membranes were  
25  
26 enhanced after the incorporation of CNCs.<sup>4, 25</sup> Although the CNC nanocomposite membranes  
27  
28 can achieve excellent water flux and antifouling performance, the antibacterial properties still  
29  
30 need to be improved. This is due to the biodegradability of CNCs, which might be beneficial  
31  
32 to the environment, but it may raise a membrane longevity concern as the thin film with  
33  
34 CNCs may interact with bacteria and will degrade during membrane filtration.<sup>26</sup> To promote  
35  
36 the antibacterial performance of membranes, a classical method is to incorporate the silver  
37  
38 nanoparticles (Ag NPs), one of the most effective bactericidal NPs with broad-spectrum  
39  
40 anti-microbial effects on bacteria, viruses, and fungi.<sup>27, 28</sup> Recent studies have employed  
41  
42 different methods to incorporate Ag NPs into membranes, including coating, adsorption and  
43  
44 covalent binding.<sup>29</sup> However, some of these methods use excess amount of Ag NPs, bringing  
45  
46 in aggregation and leaching problems which not only weaken the antibacterial performance  
47  
48 of membranes, but also lead to potential environmental hazard.<sup>29</sup> Thus, the hydrophilic CNCs  
49  
50  
51  
52  
53  
54  
55  
56  
57  
58  
59  
60

1  
2  
3  
4 with high surface area would be a good carrier to help the immobilization of Ag NPs.<sup>30</sup>  
5  
6 Besides, the electrostatic interactions between CNCs and Ag<sup>+</sup> could help the uniform growth  
7  
8 and distribution of Ag NPs on CNC surface.<sup>31</sup> Hence, we hypothesized that by combining the  
9  
10 advantages of highly hydrophilic CNCs and anti-microbial Ag NPs, CNC/Ag  
11  
12 nanocomposites are particularly suitable as an additive for TFC NF membranes.  
13  
14  
15

16  
17 Here, we reported a novel multifunctional CNC/Ag TFN NF membrane with excellent  
18  
19 performance in water flux, salt rejection, antifouling, and antibacterial properties, by  
20  
21 combining the advantages of both CNCs and Ag NPs. The CNC/Ag nanocomposites were  
22  
23 synthesized from a scalable, facile one-step reaction at room temperature, and then  
24  
25 incorporated into the active layer with different loadings. Then, the membrane characteristics,  
26  
27 water flux, desalination, antifouling and antibacterial performance were thoroughly  
28  
29 investigated. All CNC/Ag incorporated membranes showed significantly enhanced water flux  
30  
31 while remaining high rejections, as well as excellent fouling resistance and antibacterial  
32  
33 performance. Especially, the CNC/Ag-0.01 membrane reached a high water flux of 25.4 L  
34  
35 m<sup>-2</sup> h<sup>-1</sup> bar<sup>-1</sup>, high Na<sub>2</sub>SO<sub>4</sub> rejection of 99.1 %, flux recovery ratio of 92.6 % (humic acid as a  
36  
37 model foulant) and near perfect antibacterial performance (99.4 % reduction of *Escherichia*  
38  
39 *coli* viability). In addition, Ag<sup>+</sup> leaching tests proved the strong stability of CNC/Ag  
40  
41 nanocomposites in the thin film nanocomposite membranes, which not only ensures longer  
42  
43 durability of the CNC/Ag membrane but also mitigates the potential hazardous risks pose to  
44  
45 the environment.  
46  
47  
48  
49  
50  
51  
52  
53  
54  
55  
56  
57  
58  
59  
60

## 2. Experimental Methods

### 2.1 Materials and Chemicals.

PES (polyethersulfone) ultrafiltration membrane (pore size 200 nm) was acquired from Sterlitech Corp. (Kent, WA, USA). Cellulose nanocrystals (CNCs) powder was supplied by the University of Maine Process Development Center (Orono, ME, USA). Silver nitrate ( $\text{AgNO}_3$ , >99.0%), Sodium tetrahydridoborate ( $\text{NaBH}_4$ , >98.0%), 1, 3, 5-benzenetricarbonyl trichloride (TMC, purity >98.0%), piperazine (PIP, purity > 99%), sodium phosphate ( $\text{Na}_3\text{PO}_4$ , purity > 96.0%), sodium sulfate ( $\text{Na}_2\text{SO}_4$ ), sodium chloride (NaCl) and humic acid sodium salt were purchased from MilliporeSigma (Burlington, MA, USA) and used without further purifications. Deionized water (25 °C) was treated by Thermo Fisher Scientific (Waltham, MA, USA) water purification systems and used in all experiments.

### 2.2 Preparation and Characterization of CNC/Ag Nanocomposites and NF Membranes

#### 2.2.1 Preparation and Characterization of CNC/Ag Nanocomposites

The CNC/Ag nanocomposites were prepared following the method of Liu et al.<sup>30</sup> Fig. 1 presents the schematic of the synthesis of CNC/Ag nanocomposites and the fabrication of CNC/Ag TFN NF membranes. In a typical experiment, 300 mg CNCs were dispersed into 30 mL of DI water by 30 min ultrasonication to obtain a uniform 1 wt% CNC water suspension. 20 mL of 0.01 M  $\text{AgNO}_3$  solution was then mixed with the CNC water suspension and subjected to vigorous stirring for 1 h. Then, 1 mL of 0.01 M  $\text{NaBH}_4$  solution was added dropwise into the CNC/ $\text{AgNO}_3$  suspension to prepare CNC/Ag nanocomposites. After another 1 h stirring, the suspension was centrifuged at 10000 rpm for 20 min, and the bottom

1  
2  
3  
4 solids were collected and re-dispersed with DI water. The aforementioned  
5  
6  
7  
8  
9  
10  
11  
12  
13  
14  
15  
16  
17  
18  
19  
20  
21  
22  
23  
24  
25  
26  
27  
28  
29  
30  
31  
32  
33  
34  
35  
36  
37  
38  
39  
40  
41  
42  
43  
44  
45  
46  
47  
48  
49  
50  
51  
52  
53  
54  
55  
56  
57  
58  
59  
60

centrifugation-dispersion process was repeated 3 times to thoroughly wash the CNC/Ag nanocomposites. Finally, the suspension of the CNC/Ag nanocomposites was freeze-dried to yield a dry CNC/Ag nanocomposites powder. The morphology and size of the CNC/Ag nanocomposites powder were characterized by scanning electron microscopy (SEM, Hitachi SU 8010, Tokyo, Japan) at 5 kV. Samples for the SEM characterization were prepared by dispersing CNCs or CNC/Ag nanocomposites in DI water at the concentration of 0.025 wt% and then sonicate for 15 min. Afterward, a 5  $\mu$ L of sonicated suspension was further diluted by 5 mL of DI water and sonicated for 5 min. Then a 5  $\mu$ L of the prepared sample solution was dropped on the silicon wafer and air dried before characterization. The CNC sample was coated with gold for 30 s with a sputter coater (Quorum Technologies, Laughton, UK) to prevent charging of the CNC sample. Besides, the chemical compositions of CNCs and CNC/Ag composites were analyzed by X-ray Photoelectron Spectroscopy equipped with a

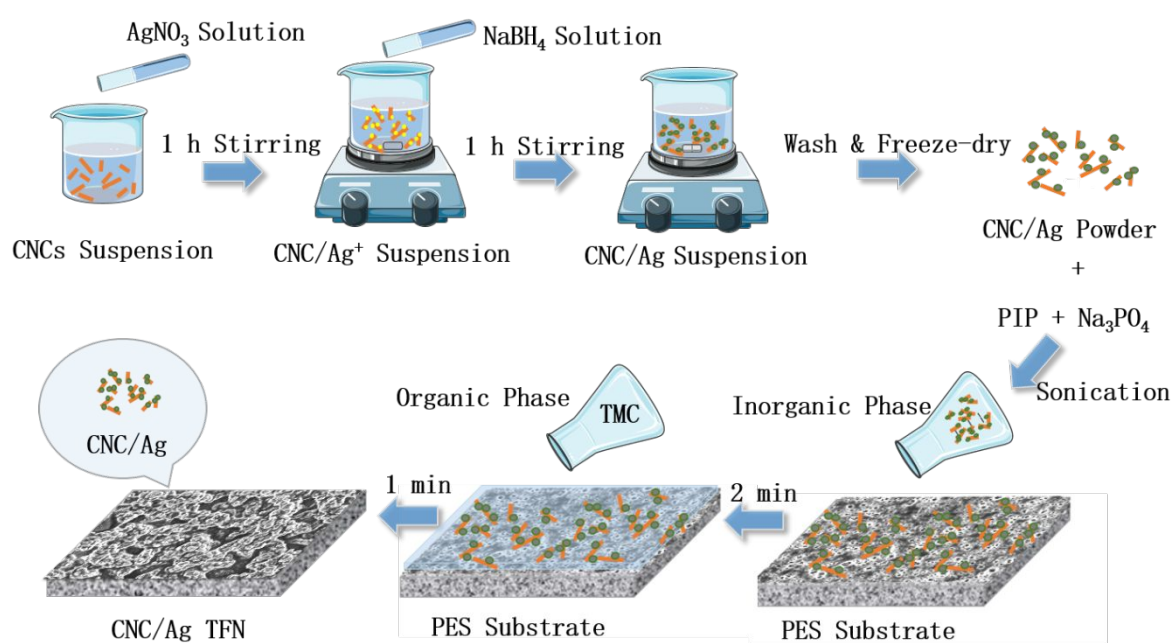


**Fig. 1** Schematic of the synthesis of CNC/Ag nanocomposites and the fabrication of CNC/Ag TFN NF membranes.

1  
2  
3  
4 flood gun (XPS, Thermo K-Alpha, Thermo Fisher Scientific, Waltham, MA, USA). The  
5  
6 presence of CNCs and Ag NPs was also attested by X-ray diffraction (XRD) (Malvern, UK).  
7  
8  
9

### 10 **2.2.2 Preparation and characterization of TFC and TFN NF Membranes**

11  
12  
13 The TFC and TFN NF membranes were prepared on the surface of commercial PES  
14  
15 membranes via the interfacial polymerization (IP) method. PES was selected as the support  
16  
17 material for the PA active layer due to its excellent chemical and thermal stability and great  
18  
19 hydrophilicity.<sup>32, 33</sup> PES substrates were immersed in DI water to get saturated for at least 20  
20  
21 min, and then the surface water on the substrates was thoroughly removed with a rubber  
22  
23 roller before the IP process. Afterward, the PES substrates were taped on the bottom of a  
24  
25 glass plate. To prepare the NF membranes, the solution containing 2.0 wt% piperazine (PIP)  
26  
27 and 0.6 wt% Na<sub>3</sub>PO<sub>4</sub> in DI water was used as the inorganic phase to pour onto the PES  
28  
29 substrate and immersed for 2 min. The excess solution was removed, and the membranes  
30  
31 were air-dried in room temperature for 10 min until no water drops on the surface. Then, the  
32  
33 PES substrates were immersed in the organic phase, which contains 0.5 wt% 1, 3,  
34  
35 5-benzenetricarbonyl trichloride (TMC) in n-hexane for 1 min. After the formation of thin  
36  
37 polyamide layer on the surface, the PES support membranes were cured in an oven at 50 °C  
38  
39 for 10 min for further polymerization. The as-synthesized TFC NF membranes were stored in  
40  
41 the refrigerator at 4 °C before testing. The TFN membranes were synthesized via the same  
42  
43 method. Various amounts of the CNC/Ag nanocomposites (0.005, 0.01, 0.02, 0.04 wt%) were  
44  
45 added into the DI water and sonicated for 20 min. Then 2.0 wt% piperazine (PIP) and 0.6  
46  
47 wt% Na<sub>3</sub>PO<sub>4</sub> were added into the CNC/Ag suspension and sonicated for 20 min to prepare  
48  
49  
50  
51  
52  
53  
54  
55  
56  
57  
58  
59  
60

the inorganic phase. After the IP process, CNC/Ag-0.005, CNC/Ag-0.01, CNC/Ag-0.02, and CNC/Ag-0.04 NF membranes were synthesized, respectively. Besides, 0.01 wt% CNC (without Ag) was added into the inorganic phase to get the CNC-0.01 NF membrane. The fabrication conditions of the synthesized membranes in this study are presented in Table 1.

**Table 1.** The fabrication conditions for the synthesized membranes.

Membrane Type	PIP (wt%)	TMC (wt%)	CNC (wt%)	CNC/Ag (wt%)
TFC	2.0	0.5	/	/
CNC-0.01	2.0	0.5	0.01	/
CNC/Ag-0.005	2.0	0.5	/	0.005
CNC/Ag-0.01	2.0	0.5	/	0.01
CNC/Ag-0.02	2.0	0.5	/	0.02
CNC/Ag-0.04	2.0	0.5	/	0.04

All membranes were dried at room temperature before characterization. Fourier transform infrared (FT-IR) spectrometer (Spectrum 400, PerkinElmer, Waltham, MA, USA) was employed to study the FT-IR spectra of the near-surface region chemical composition of NF membranes. The element composition of membranes was analyzed by XPS (Thermo Fisher Scientific, Waltham, MA, USA). The surface morphology of the as-synthesized membranes was analyzed by SEM at 5 kV. Membrane samples were coated with gold for 30 s with a sputter coater (Quorum Technologies, Laughton, UK) to prevent charging of the membrane surface. The hydrophilicity of membranes was studied by a contact angle goniometer (Model 250, Ramé-Hart Instrument Co., Netcong, NJ, USA). Atomic force microscopy (AFM) (Agilent 5500, Agilent Technologies, Inc., Santa Clara, CA, USA) was employed to measure the surface roughness of the as-synthesized membrane samples (tapping mode, a scan size of  $5 \times 5 \mu\text{m}^2$ , and a scan rate of 0.5 line/s).

### 2.3 Pure Water Flux and Desalination Performance Tests

The performance of the synthesized NF membranes was evaluated by a cross-flow filtration system (Fig. S1). Flux and desalination performance tests were conducted at room temperature and at a cross-flow rate of 350 mL/min. The membrane test area was 4.1 cm<sup>2</sup>. Membrane samples were stabilized with DI water at 6 bar for 1 hour to reach steady state and tested under 4.8 bar. The pure water flux  $J_w$  (L·m<sup>-2</sup>·h<sup>-1</sup> or LMH) was calculated based on eq 1.

$$J_w = \frac{V}{A\Delta t} \quad (1)$$

where  $V$  is the volume of water permeate (L),  $\Delta t$  (h) represents permeate collection time interval, and  $A$  is the effective area of tested membrane (m<sup>2</sup>).

The desalination performances of the TFC, CNC TFN, and CNC/Ag TFN NF membranes were investigated using Na<sub>2</sub>SO<sub>4</sub> and NaCl aqueous solutions at the concentration of 2000 ppm. The feed and permeate concentrations were measured with a conductivity meter (Extech Instruments Corp., Waltham, MA, USA). The salt rejection percentage  $R$  (%) was calculated using eq 2.

$$R = \left(1 - \frac{C_p}{C_f}\right) \times 100\% \quad (2)$$

where  $C_f$  is the feed concentration (mg/L), and  $C_p$  represents the permeate concentration (mg/L). Besides, water permeability  $P$  was calculated by  $P = J_w/\Delta P$ , where  $\Delta P$  stands for the transmembrane pressure (TMP) in bars. All the flux and rejection of the tested membranes were measured three times with three individual membrane samples.

## 2.4 Antifouling Performance

The antifouling performance was evaluated using 500 ppm humic acid as a model foulant for the TFC, CNC TFN, and CNC/Ag TFN NF membranes. The antifouling test was conducted under the TMP of 4.8 bar at a cross-flow rate of 350 mL/min. Membranes were first stabilized under 6 bar TMP for 1 hour using DI water to reach the steady state, and the initial water flux ( $J_{w0}$ ) was recorded. Then the feed solution was replaced with 500 ppm humic acid solution immediately. Afterward, the permeate flux ( $J_{wr}$ ) was recorded continuously for 4 hours. Then the feed solution was changed to DI water to flush the membrane test system and membrane surface for 30 min under the cross-flow rate of 350 mL/min. After flushing, the water flux ( $J_{wr}$ ) after the fouling experiment was retested under the same TMP and recorded. The normalized flux ( $J_{wr}/J_{w0}$ ) and flux recovery ratio ( $FRR$ , %) were calculated to represent the antifouling properties of the NF membranes.  $FRR$  was calculated using  $FRR = J_{wr}/J_{w0} * 100\%$ , which represents the flux after the antifouling test comparing with the original flux.<sup>3, 34, 35</sup>

## 2.5 Antibacterial Activity Measurement of Membranes

The antibacterial properties of the NF membranes synthesized in this study were tested using Gram-negative *Escherichia coli* (*E. coli*, ATCC 10798) as the model bacteria following the colony forming unit (CFU) counting method reported in the previous literature.<sup>36, 37</sup> Firstly, bacteria were cultured in a Luria–Bertani (LB) broth at 35 °C overnight to reach the log phase. The *E. coli* culture was centrifuged at 4000 rpm to remove supernatant and washed with DI water for 3 times. Then, the bacteria suspension was diluted to the concentration of

1  
2  
3  
4 approximately  $10^7$  CFU mL<sup>-1</sup> with 0.9% NaCl. After that, a 5 cm<sup>2</sup> membrane coupon was cut  
5  
6 and fixed in a glass holder to expose only the NF active layer to bacteria. Then the membrane  
7  
8 surface was soaked with 10 mL of bacteria solution for 3 h at room temperature. The excess  
9  
10 solution was then discarded, and the surface of the membrane coupon was washed with 5 mL  
11  
12 of 0.9% saline solution to remove loosely attached bacteria. The membrane coupon was then  
13  
14 put into a small beaker with 10 mL 0.9% saline solution and sonicate (Branson CPX3800  
15  
16 Ultrasonic Bath, 40 kHz, 110 W) for 10 min to remove bacteria attached on membrane  
17  
18 surface. Finally, the bacteria solution was diluted and spread on LB agar plates. After 12 h  
19  
20 incubation at 35 °C, CFU was counted for each plate. This method effectively illustrates the  
21  
22 antibacterial performance of membranes by assessing the ability to inhibit biofilm growth on  
23  
24 membrane surface. The bacterial viability was also calculated by the following equation:  
25  
26  
27  
28  
29  
30  
31  
32

$$\text{Bacterial viability} = \frac{N}{N_0} \times 100\% \quad (4)$$

33  
34  
35  
36  
37  
38 where  $N$  and  $N_0$  are the colony counts corresponding to the NP modified membranes and the  
39  
40 TFC NF membrane, respectively. Meanwhile, a fluorescence microscope (Zeiss, Oberkochen,  
41  
42 Germany) was employed to study live and dead bacteria on the membrane surface after 3 h  
43  
44 incubation of *E. coli*. After the incubation, membrane coupons were rinsed with 5 mL of 0.9%  
45  
46 NaCl solution to remove loosely attached bacteria and then incubated for another 1 h. Then  
47  
48 membrane coupons were stained with SYTO 9 (1.67 mM) and propidium iodide (PI, 15 mM)  
49  
50 for 15 min in the dark. Finally, images were attained by the fluorescence microscope.  
51  
52  
53  
54  
55

## 56 **2.6 Silver ions releasing test of the CNC/Ag-TFN NF Membranes**

57  
58 The releasing rate of silver ions (Ag<sup>+</sup>) from the CNC/Ag NF membranes were measured  
59  
60

1  
2  
3  
4 following the protocol reported by other studies.<sup>38</sup> The 5 cm<sup>2</sup> CNC/Ag NF membrane coupon  
5  
6 was soaked in a beaker with 20 mL of DI water at room temperature (25 °C) stirring at 50  
7  
8 rpm on a rotator. The solution was collected every 24 h for 10 days and replaced with fresh  
9  
10 DI water. All collected solutions were acidified with 2.0 wt% HNO<sub>3</sub> solution and then  
11  
12 analyzed Ag content by inductively coupled plasma optical emission spectrometry (ICP-OES,  
13  
14 PerkinElmer, Waltham, MA). Besides, another 5 cm<sup>2</sup> CNC/Ag NF membrane coupon was  
15  
16 soaked into 20 mL of 2.0 wt% HNO<sub>3</sub> solution and sonicated for 20 min to totally dissolve all  
17  
18 Ag NPs incorporated in the membrane surface. The total amount of silver was determined by  
19  
20 ICP-OES as well.  
21  
22  
23  
24  
25

### 26 27 **3 Results and Discussion**

#### 28 29 **3.1 Characterization of CNC/Ag Nanocomposites**

30  
31  
32 The properties of CNCs and CNC/Ag nanocomposites were characterized by SEM, XPS, and  
33  
34 XRD. The morphology of the CNCs and the CNC/Ag nanocomposites from a dilute water  
35  
36 suspension were overserved by SEM (Fig. 2). As shown in Fig. 2a, CNCs were in rod-like  
37  
38 shapes with the dimensions of 5-20 nm wide and 150-200 nm long (size distributions of  
39  
40 CNCs were presented in Fig. S2. With high surface area and abundant surface hydroxyl  
41  
42 groups, CNCs exhibited strong ability to absorb Ag<sup>+</sup> stably and uniformly.<sup>30, 31</sup> After the  
43  
44 treatment with NaBH<sub>4</sub> solution, the presence of Ag NPs can be seen from Fig. 2b with a  
45  
46 diameter of around 50 nm attached to the CNC surface, indicating that CNC/Ag  
47  
48 nanocomposites were synthesized successfully. As the Ag<sup>+</sup> mobility was decreased by its  
49  
50 interactions with CNC's hydroxyl groups, the growth of large Ag NPs were prevented and  
51  
52 the stabled Ag NPs can be formed on CNC surface.<sup>27</sup>  
53  
54  
55  
56  
57  
58  
59  
60

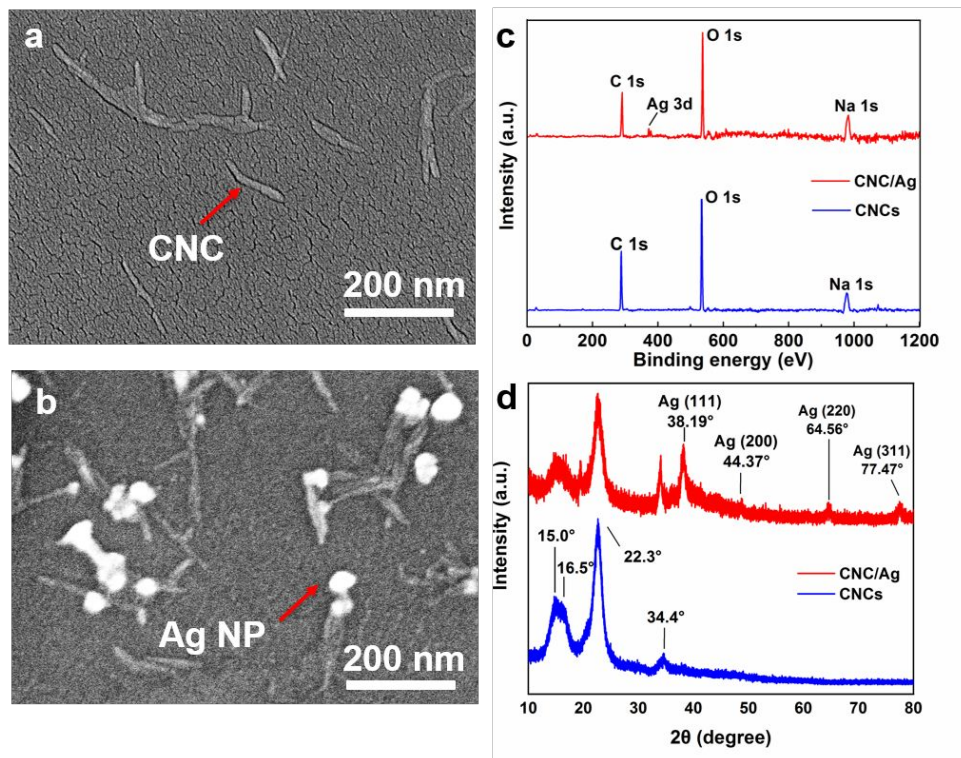


**Fig. 2** Characterization of CNCs and CNC/Ag nanocomposites. (a) SEM image of CNCs, (b) SEM image of CNC/Ag nanocomposites, (c) XPS survey spectrum of CNCs and CNC/Ag nanocomposites, and (d) XRD results of CNCs and CNC/Ag nanocomposites.

The XPS survey spectrum in Fig. 2c shows the presence of C, N, and Ag in the as-synthesized nanocomposite, and the Ag 3d peak around 368.2 eV further demonstrated the presence of Ag in the oxidation state of zero.<sup>39</sup> The presence of Ag NPs was also confirmed by the XRD results. Fig. 2d presents peaks at 38.19°, 44.37°, 64.56°, and 77.47°, in correspondence with the diffraction peaks from the (111), (200), (220), and (311) planes of silver metal NPs, respectively.<sup>40</sup> Besides, the XRD peaks of CNCs at 15°, 16.5°, 22.3°, and 34.4° reflect the ( $1\bar{1}0$ ), (110), (200), and (004) planes of cellulose, respectively.<sup>4</sup>

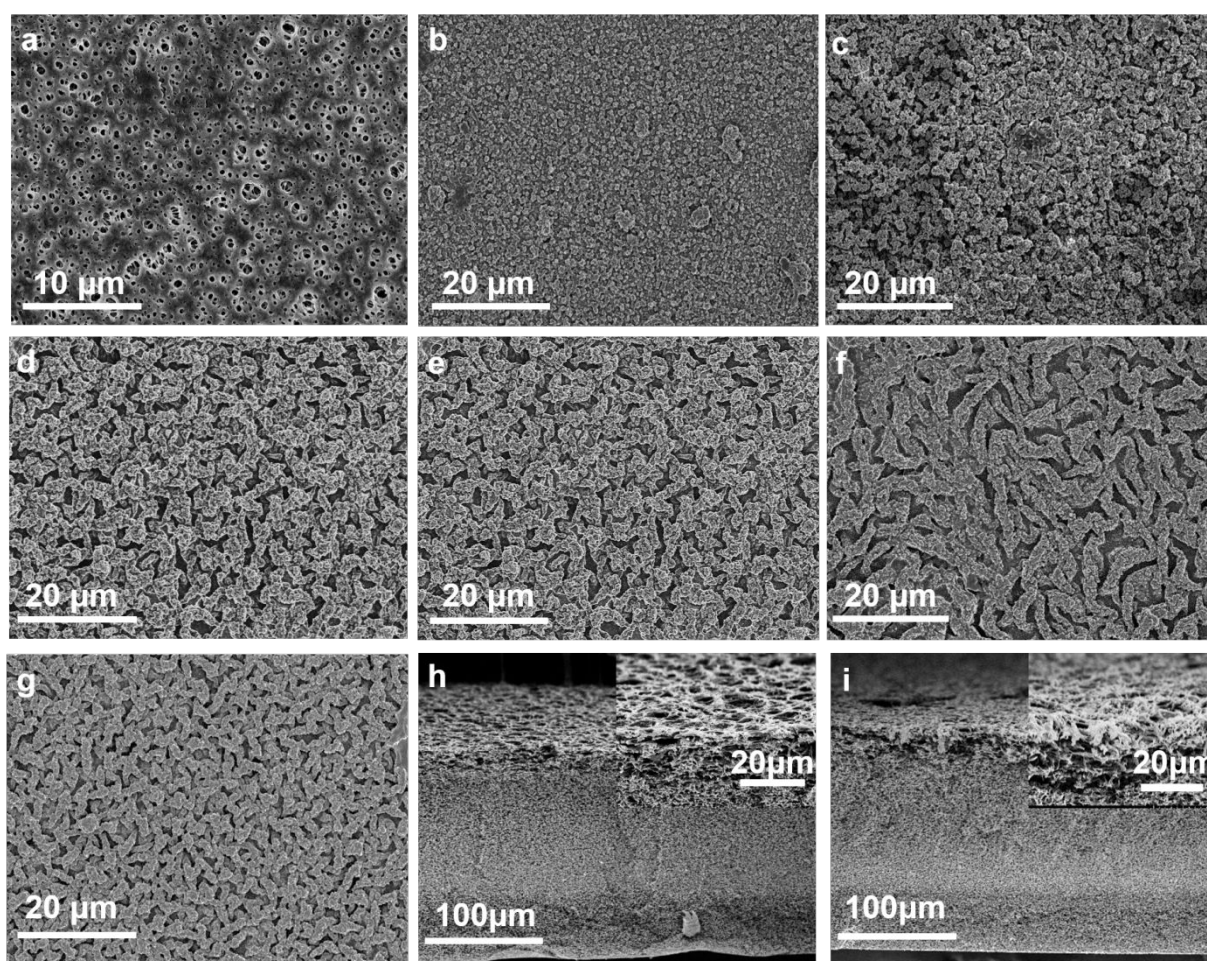
### 3.2 Characterization of NF Membranes

**Characterization of Membrane Surface Chemistry.** FT-IR analysis was conducted to analyze the functional groups on the membrane surface, and the results were depicted in Fig.

1  
2  
3  
4 S3. The peak at  $1625\text{ cm}^{-1}$  is related to C=O stretching vibration, confirming the formation –  
5  
6 CO-NH- group during the IP process.<sup>41</sup> The peak at approximately  $1420\text{ cm}^{-1}$  is ascribed to  
7  
8 the O-H stretching vibration, which may be related to the carboxyl groups generated via the  
9  
10 hydrolysis of the unreacted acyl chlorides during the IP process.<sup>42</sup> The characteristic peak  
11  
12 around  $3400\text{ cm}^{-1}$  is the typical O-H stretching vibration in carboxyl introduced by IP process  
13  
14 and the absorption of unreacted -NH.<sup>3, 43</sup> The aforementioned peaks confirmed the successful  
15  
16 formation of polyamide thin active layer. However, no obvious characterization peaks of  
17  
18 CNCs were observed in Fig. S3a, which could be explained by the low concentrations of  
19  
20 CNCs and CNC/Ag nanocomposites as the peaks may be covered by strong peaks of  
21  
22 polyamide.<sup>3, 4, 44</sup> Furthermore, Ag 3d XPS spectrum confirmed the existence of Ag NPs on  
23  
24 CNC/Ag TFN membrane surface as Fig. S3b exhibits two different peaks Ag  $3d_{3/2}$  at 374.5  
25  
26 eV and Ag  $3d_{5/2}$  at 368.5 eV, which are typical peaks of Ag NPs.<sup>45, 46</sup>  
27  
28  
29  
30  
31  
32  
33  
34

35 **Membrane Surface Morphology Characterization.** The surface morphology of all  
36  
37 synthesized NF membranes was investigated by both SEM (Fig. 3) and 3 D AFM (Fig. 4).  
38  
39 Compared with the SEM image of PES support (Fig. 3a), the TFC NF membrane depicted  
40  
41 uniform nodular structure, which is the typical surface morphology of polyamide layer (Fig.  
42  
43 3b), indicating the substrate was fully covered by the active layer. After adding CNC/Ag  
44  
45 nanocomposites, the surface exhibited a different structure as ridges and valleys (Fig. 3c to  
46  
47 Fig. 3f), which was similar to the surface structures observed by Tan et al.<sup>47</sup> in their study of  
48  
49 nanoscale Turing structures of polyamide membranes. The relatively rough and  
50  
51 non-homogeneous Turing structures also increased the surface roughness of NF membranes  
52  
53 after the incorporation of CNC/Ag nanocomposites into the thin active layer (Fig. 4).<sup>47</sup> The  
54  
55  
56  
57  
58  
59  
60

1  
2  
3  
4 incorporation of hydrophilic CNC/Ag nanocomposites could increase the hydrophilicity of  
5  
6 inorganic phase, thus reduced the diffusion of piperazine (PIP) from inorganic phase to  
7  
8 organic phase during the reaction process and resulted in rougher surface morphology.<sup>47, 48</sup>  
9  
10  
11 The striped Turing structure was mainly caused by the interaction of CNCs with the excess  
12  
13 TMC by hydrogen bonding in self-inhibition process during the interfacial polymerization.<sup>3,</sup>  
14  
15  
16  
17 <sup>49</sup> This was further confirmed by adding the same percentage of CNCs into the active layer as  
18  
19 a similar ridge-and-valley surface structure was observed from the CNC-0.01 NF membrane  
20  
21  
22 (Fig. 3g).<sup>35</sup>  
23  
24  
25  
26



57  
58 **Fig. 3** Surface SEM images of (a) PES substrate (b) the TFC, (c) CNC/Ag-0.005, (d)  
59 CNC/Ag-0.01, (e) CNC/Ag-0.02, and (f) CNC/Ag-0.04, and (g) CNC-0.01 NF membranes.  
60 Cross sectional SEM images of the (h) TFC and (i) CNC/Ag-0.01 NF membranes.

Besides, the surface roughness increased gradually from  $S_q=151.5$  nm (Fig. 4c) to 329.5 nm (Fig. 4f) with the addition of CNC/Ag nanocomposites amount increased from 0.005 wt% to 0.04 wt%, which is consistent with the surface structure changes (Fig. 3). With the increasing amounts of CNC/Ag nanocomposites in inorganic phase, the viscosity of aqueous phase could be higher, which would further limit the diffusion of PIP at the interface and led to a higher roughness.<sup>18</sup> In addition, the increased surface roughness (Fig. 4) and the cross-sectional images of TFC (Fig. 3h) and CNC/Ag-0.01 (Fig. 3i) NF membranes also confirmed the successful synthesis of polyamide thin active layers on the PES substrates.

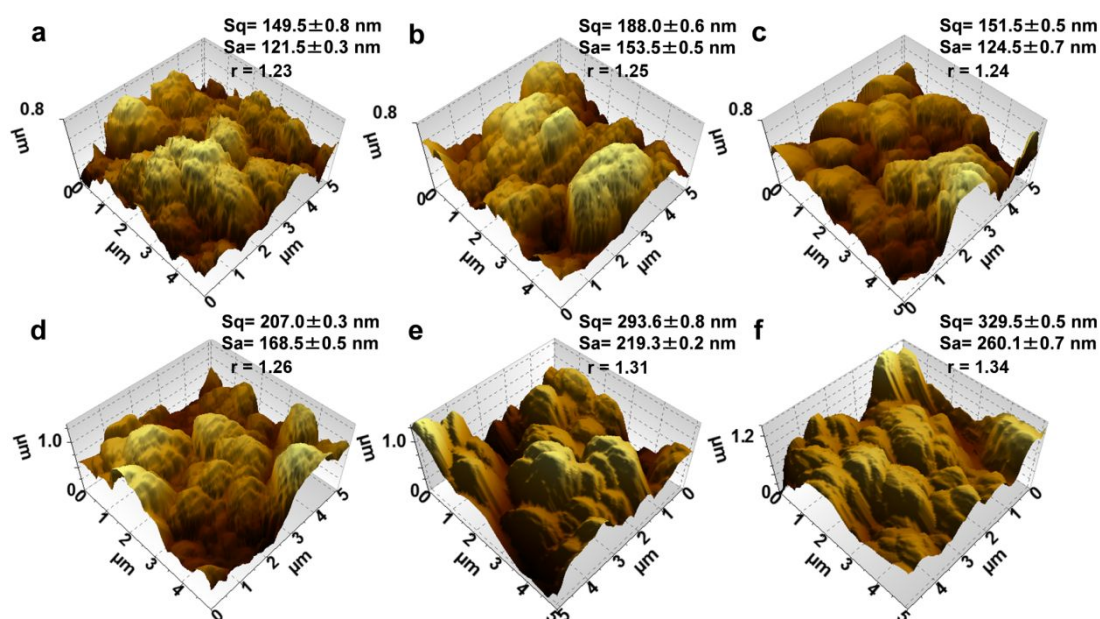


**Fig. 4** AFM images of (a) the TFC, (b) CNC-0.01, (c) CNC/Ag-0.005, (d) CNC/Ag-0.01, (e) CNC/Ag-0.02, and (f) CNC/Ag-0.04 membrane surface, where  $S_q$  represents Root Mean Square Height,  $S_a$  stands for Arithmetical Mean Height and  $r$  represents roughness ratio (the ratio of true area of the solid surface to the apparent area).

### 3.3 Pure Water Permeability and Salt Rejection Performance

The trade-off of permeability and selectivity has been a critical problem that limits the improvement of the energy efficiency and separation performance upper bound during the

1  
2  
3  
4 water treatment process. Thus, the pure water permeability and salt rejection performance of  
5  
6 CNC/Ag NF membranes were both evaluated. The pure water permeability measured under  
7  
8 4.8 bar at room temperature for the TFC, CNC TFN, and CNC/Ag TFN NF membrane can be  
9  
10 seen from Fig. 5a. All NF membranes achieved higher pure water permeability after the  
11  
12 addition of CNC/Ag nanocomposites. The following sequence of water permeability was  
13  
14 observed: CNC/Ag-0.01 > CNC/Ag-0.02  $\approx$  CNC/Ag-0.04 > CNC/Ag-0.005 > TFC NF. The  
15  
16 highest pure water permeability (25.4 LMH/bar) was achieved by the CNC/Ag-0.01  
17  
18 membrane, which was 1.6 times higher than the TFC membrane. The significant  
19  
20 enhancement of pure water flux can be due to the improved membrane hydrophilicity after  
21  
22 the addition of hydrophilic CNC/Ag nanocomposites in PA active layer.<sup>2-5</sup> The water contact  
23  
24 angle was measured to assess the membrane hydrophilicity, as shown in Fig. 5b. After the  
25  
26 incorporation of CNC/Ag nanocomposites, the water contact angles of all CNC/Ag NF  
27  
28 membranes were lower than that of the pristine TFC NF membrane (37.3°). As smaller water  
29  
30 contact angles indicate more hydrophilic surfaces, the hydrophilicity of all CNC/Ag NF  
31  
32 membranes was improved after the addition of CNC/Ag nanocomposites. Besides, the trend  
33  
34 of the membrane hydrophilicity was observed to be in accordance with that of the water  
35  
36 permeability, which implies the strong impact of membrane hydrophilicity on membrane  
37  
38 flux. The best hydrophilicity was the CNC/Ag-0.01 membrane with the contact angle of  
39  
40 18.7°, which was almost 50% lower than that of the TFC NF membrane. Besides membrane  
41  
42 hydrophilicity, the increase of membrane surface roughness could also contribute to the  
43  
44 increased membrane flux.<sup>6, 7</sup> According to the Wenzel theory ( $\cos \theta_m = r * \cos \theta$ , where  $\theta$   
45  
46 represents Young contact angle,  $r$  is the roughness ratio, and  $\theta_m$  stands for the measured  
47  
48  
49  
50  
51  
52  
53  
54  
55  
56  
57  
58  
59  
60

1  
2  
3  
4 contact angle), for a hydrophilic ideal surface, the larger the roughness ratio  $r$ , the more  
5  
6 influence of roughness on membrane surface properties.<sup>8</sup> However, our calculated results of  $r$   
7  
8 (Fig. 4) shows that there were no significant differences between  $r$  for the blank sample and  
9  
10 the membranes with different CNC/Ag loadings, indicating the minor influence of surface  
11  
12 roughness on the improvement of water flux compared with the influence of membrane  
13  
14 hydrophilicity. Therefore, when the loading of CNC/Ag nanocomposites increased from 0 to  
15  
16 0.01 wt%, the pure water flux was improved as the membrane hydrophilicity and surface  
17  
18 roughness increased simultaneously. When the loadings of CNC/Ag nanocomposites were  
19  
20 higher than 0.01 wt% (CNC/Ag-0.02 and CNC/Ag-0.04 membranes), although the surface  
21  
22 roughness became larger, their hydrophilicity decreased according to the measured contact  
23  
24 angles. Consequently, their membrane flux was lower than that of the CNC/Ag-0.01  
25  
26 membrane as the membrane intrinsic hydrophilicity played a dominant role rather than  
27  
28 surface roughness.  
29  
30  
31  
32  
33  
34  
35  
36

37  
38 The desalination performance of all as-synthesized NF membranes was evaluated by 2000  
39  
40 ppm  $\text{Na}_2\text{SO}_4$  and NaCl in this study. The trends of the water permeability in Fig. 5c and Fig.  
41  
42 5d were in consistent with that of the pure water permeability in Fig. 5a. Compared with the  
43  
44 pristine TFC NF membrane, the water permeability of CNC/Ag-0.01 membrane increased  
45  
46 from 11 LMH/bar to 13.6 LMH/bar for  $\text{Na}_2\text{SO}_4$ . In the meantime, the CNC/Ag-0.01  
47  
48 membrane also maintained a high  $\text{Na}_2\text{SO}_4$  rejection rate of 99.1%. In addition, the water  
49  
50 permeability of the TFN NF membrane was enhanced from 14.7 LMH/bar to 22.4 LMH/bar  
51  
52 for NaCl after the addition of 0.01 wt% CNC/Ag nanocomposites. The rejection of NaCl  
53  
54 slightly increased from 21 % (the TFC membrane) to 23.4 % (CNC/Ag-0.01). The rejection  
55  
56  
57  
58  
59  
60

1  
2  
3  
4 rate of NaCl was much lower than Na<sub>2</sub>SO<sub>4</sub> as the hydration ions radii of Cl<sup>-</sup> (0.1 nm) is  
5  
6  
7  
8  
9  
10  
11  
12  
13  
14  
15  
16  
17  
18  
19  
20  
21  
22  
23  
24  
25  
26  
27  
28  
29  
30  
31  
32  
33  
34  
35  
36  
37  
38  
39  
40  
41  
42  
43  
44  
45  
46  
47  
48  
49  
50  
51  
52  
53  
54  
55  
56  
57  
58  
59  
60

smaller than  $\text{SO}_4^{2-}$  (0.3 nm).<sup>18</sup> Thus, it is much easier for  $\text{Cl}^-$  to pass through polyamide layer than that of  $\text{SO}_4^{2-}$ .<sup>18</sup> CNC/Ag-0.01 membrane exhibited outstanding desalination properties in both water permeability and salt rejection. This could be attributed to the relatively high water permeability sites on the striped Turing structure, breaking through the upper limit of the permeability-selectivity trade-off for this CNC/Ag TFN membrane.<sup>47</sup> Besides, the cross-linking degree could be higher after the addition of CNC/Ag nanocomposites, which would be beneficial to maintain high salt rejections for TFN membranes.<sup>3</sup>

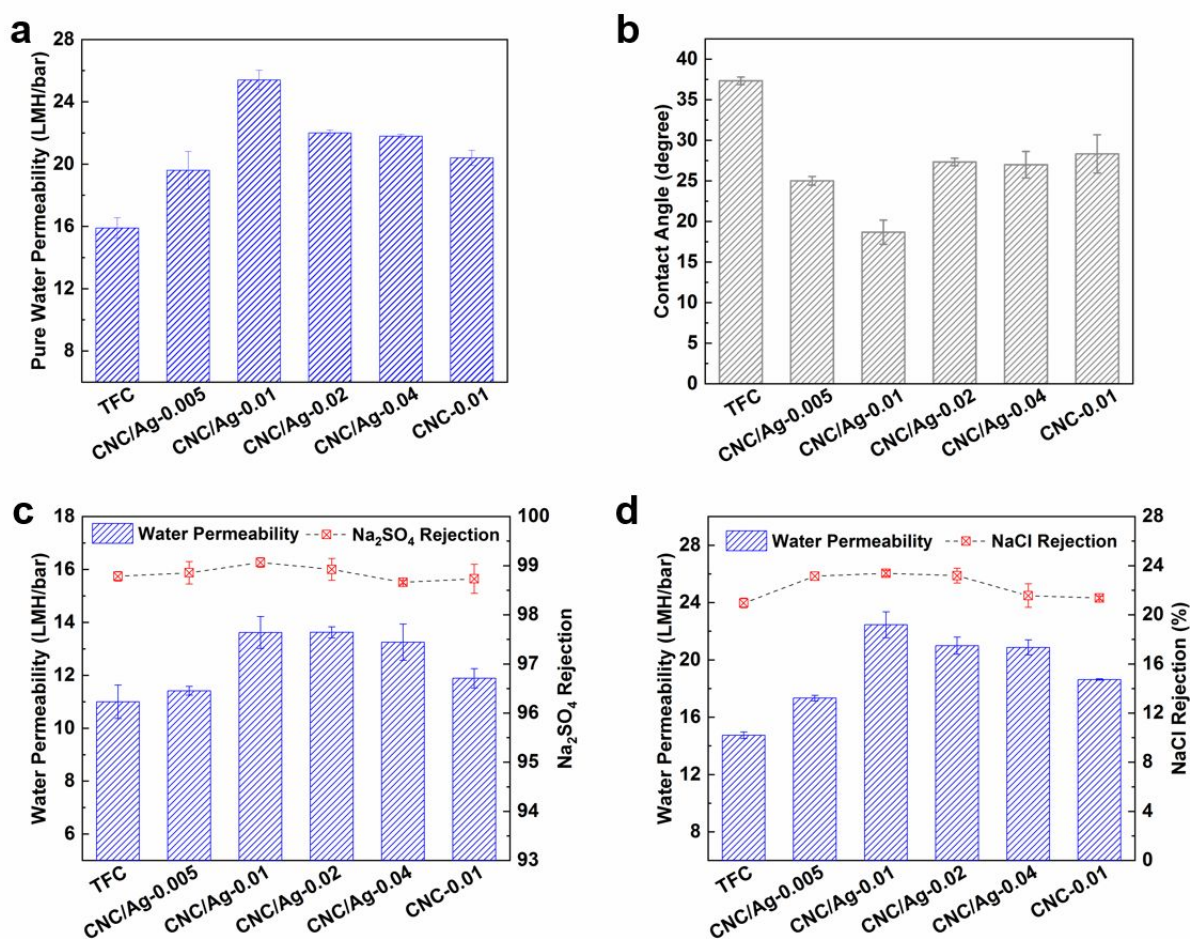


**Fig. 5** (a) Pure water permeability, (b) water contact angle, (c)  $\text{Na}_2\text{SO}_4$  permeability and rejection, (d)  $\text{NaCl}$  permeability and rejection of the membranes under 4.8 bar. The salt concentrations used are 2000 ppm.

### 3.4 Antifouling and Antibacterial Performance of Membranes

#### 3.4.1 Humic Acid Antifouling Performance

Membrane fouling is a major threat to long-term NF operations. Common membrane foulants include inorganic, organic, colloidal and biological foulants, which will not only decline the water flux but also impair the membrane durability in long-term operations.<sup>54, 55</sup> In this study, the antifouling properties of the CNC/Ag TFN membranes were firstly investigated using humic acid, a typical natural organic matter (NOM),<sup>3, 49, 54</sup> with a concentration of 500 ppm. Fig. 6 shows the normalized flux with time (Fig. 6a) and flux recovery ratio (FRR, %, Fig. 6b). Typically, a higher FRR value represents a better antifouling property of the tested membrane. All CNC/Ag membranes presented a much higher FRR than the TFC NF membrane (Fig. 6b). Especially, CNC/Ag-0.01 reached the highest FRR of 92.6 %, which was ~37 % higher than that of the TFC NF membrane and ~10% higher than that of the CNC-0.01 TFN membrane. The enhanced antifouling performance of CNC/Ag NF membranes could be explained by the introduction of hydrophilic CNC/Ag nanocomposites into the polyamide layer, which could help mitigate fouling by weakening the interactions with the hydrophobic humic acid molecules.<sup>35, 56</sup> Also, the abundant hydroxyl groups on CNC surface could act as active sites that are available for hydrogen bonds to form a hydration layer on membrane surface, thus reducing the attachment of foulants.<sup>57</sup> However, the CNC/Ag-0.02 and CNC/Ag-0.04 membranes presented lower FRR than that of the CNC/Ag-0.01 membrane. According to studies conducted by previous researchers, low surface roughness enhanced the antifouling performance of membranes because of the

suppressed attachment tendency of foulants on the smooth active layer.<sup>15, 57</sup> Thus, with the incorporation of more than 0.01 wt% of CNC/Ag nanocomposites, the surface roughness became larger and thus the antifouling performance for humic acid slightly decreased.

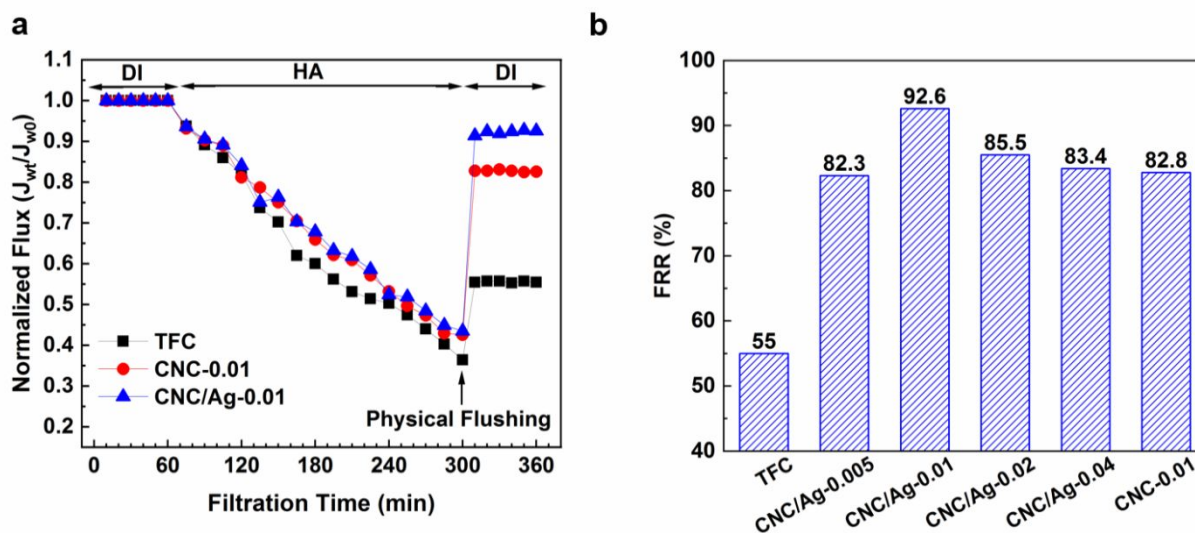


**Fig. 6** Antifouling performance of the membranes under 4.8 bar. (a) Time-dependent normalized flux and (b) Flux recovery ratio (FRR). The cross-flow rate for all pure water flux and humid acid fouling tests was 350 mL/min.

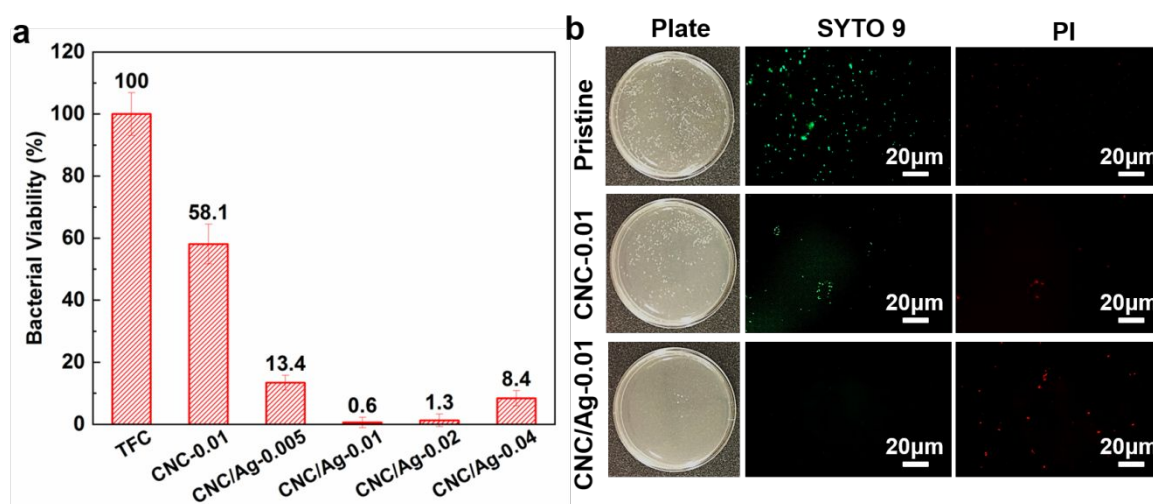
### 3.4.2 Antibacterial Performance

Besides organic fouling, biological and microbial membrane fouling will also lead to flux decline, high energy consumption, and shortened membrane life span.<sup>58</sup> To analyze the antibacterial performance of the fabricated membranes, membrane surface was exposed to the model gram-negative bacteria *E. coli* suspension for 3 h, and the colony forming unit (CFU) plate counting method was applied to determine the number of alive bacteria attached on membrane surface. Fig. 7a demonstrates that all CNC/Ag NF membranes presented excellent antibacterial performance of over 86% bacterial viability reduction. Especially, CNC/Ag-0.01 achieved the lowest bacterial viability ratio of around 0.6 % (99.4 % bacterial viability

1  
2  
3  
4 reduction), demonstrating its outstanding antibacterial performance. The excellent  
5  
6 antibacterial performance of CNC/Ag NF membranes could be mainly due to the antibacterial  
7  
8 property of CNC/Ag nanocomposites.<sup>30</sup> It is widely acknowledged that Ag is one of the most  
9  
10 effective antimicrobials, and main antibacterial mechanisms of Ag NPs include direct contact  
11  
12 cell damage, the generation of reactive oxygen species and Ag<sup>+</sup> released from Ag NPs.<sup>20, 46, 59</sup>  
13  
14 Besides the biocidal effect of Ag NPs, the excellent antibacterial performance could also be  
15  
16 attributed to the anti-attachment effect of CNC/Ag TFN membrane surface to bacteria.<sup>60</sup>  
17  
18 Enhanced hydrophilicity, low surface roughness will lower the adhesion of *E. coli* and lead to  
19  
20 different membrane antibacterial performance.<sup>45</sup> Thus, the greatly improved hydrophilicity  
21  
22 (Fig. 5b) and relatively flat membrane surface (Fig. 4) after incorporating 0.01 wt% CNC/Ag  
23  
24 nanocomposites could effectively suppress the attachment of bacteria. With the combination  
25  
26 influence of the biocidal effect from Ag NPs and the strong anti-attachment effect on bacteria,  
27  
28 the CNC/Ag-0.01 NF membrane achieved the best antibacterial performance. However, the  
29  
30 antibacterial performance of CNC/Ag NF membranes after adding more nanocomposites was  
31  
32 slightly decreased compared with CNC/Ag-0.01, which could be explained by their higher  
33  
34 surface roughness and lower hydrophilicity (Fig. 4 and Fig. 5). With higher loadings of  
35  
36 CNC/Ag nanocomposites, although the biocidal effects could be enhanced by larger amount  
37  
38 of Ag NPs, the weakened anti-attachment influence on bacteria could be the dominate reason  
39  
40 to the antibacterial performance decline of CNC/Ag-0.02 and CNC/Ag-0.04 membranes.  
41  
42  
43 In order to further analyze the antibacterial mechanism of CNC/Ag TFN membranes,  
44  
45 fluorescent microscopy (Zeiss, Oberkochen, Germany) analysis was applied and the results  
46  
47 were depicted in Fig. 7b where red dots represent dead cells and green dots indicate live cells.  
48  
49  
50  
51  
52  
53  
54  
55  
56  
57  
58  
59  
60

1  
2  
3  
4 After 3 h incubation of NF membranes in *E. coli* solution, the TFC NF membrane exhibited  
5  
6  
7  
8  
9  
10  
11  
12  
13  
14  
15  
16  
17  
18  
19  
20  
21  
22  
23  
24  
25  
26  
27  
28  
29  
30  
31  
32  
33  
34  
35  
36  
37  
38  
39  
40  
41  
42  
43  
44  
45  
46  
47  
48  
49  
50  
51  
52  
53  
54  
55  
56  
57  
58  
59  
60

1  
2  
3  
4 strong green fluorescence, and almost no dead cell was shown on the membrane surface,  
5  
6 which indicates that the TFC NF membrane did not have obviously antibacterial effect.  
7  
8 Besides, the dense green dots could also imply its bad anti-attachment effect on *E. coli*. In  
9  
10 contrast, the CNC/Ag-0.01 NF membrane achieved strong biocidal performance as well as  
11  
12 excellent anti-attachment performance, which was in consistent with the quantitative results  
13  
14 in Fig. 7a. Almost all cells on CNC/Ag-0.01 membrane surface were dead, and fewer cells  
15  
16 were observed including both dead cells and alive cells, indicating the suppression of  
17  
18 bacterial adhesion. In order to further analyze the anti-attachment effect on the overall  
19  
20 CNC/Ag membrane antibacterial performance, the antibacterial performance of CNC-0.01  
21  
22 TFN was also evaluated. CNC-0.01 membrane achieved a reduction of bacterial viability of  
23  
24 58 % (Fig. 7a), and Fig. 7b demonstrates that almost all remaining bacteria on CNC-0.01  
25  
26 membrane surface were alive, indicating that CNCs only reduce the attachment of bacteria  
27  
28 rather than exhibit biocidal performance.  
29  
30  
31  
32  
33  
34  
35  
36  
37



38  
39  
40  
41  
42  
43  
44  
45  
46  
47  
48  
49  
50  
51  
52  
53  
54 **Fig. 7** Antibacterial performance results. (a) Colony forming unit (CFU) plate counting  
55 results of all membranes, and (b) the agar plate results and fluorescence microscopy images  
56 of the pristine TFC (upper row), CNC-0.01 (middle) and CNC/Ag-0.01 (bottom) NF  
57 membranes, where the live bacteria stained with SYTO 9 (green color) and the dead bacteria  
58 stained with PI (red color).  
59  
60

### 3.5 Stability of Ag NPs in the CNC/Ag TFN Membrane

The stability of Ag NPs is known to have strong influence on the effectiveness and duration of membrane antibacterial performance.<sup>61</sup> Besides, although silver ions show low-toxicity to humans, high concentration of Ag<sup>+</sup> can still cause DNA damage to human cells.<sup>29, 61</sup> Thus, the stability of Ag NPs in CNC/Ag-0.01 TFN membrane was analyzed by the Ag<sup>+</sup> leaching experiment in this study. 5 cm<sup>2</sup> membrane coupons of the CNC/Ag-0.01 TFN membrane were immersed in a beaker with 20 mL of DI water under 50 rpm stirring for 10 consecutive days, and the Ag content was measured via ICP-OES. As illustrated in Fig. 8, the initial releasing rate was 0.0135  $\mu\text{g cm}^{-2} \text{day}^{-1}$ , and then decreased dramatically to around 0.0063  $\mu\text{g cm}^{-2} \text{day}^{-1}$  from the second day. This trend was in accordance with the observations in previously reported studies.<sup>1, 44, 46</sup> From the third day, the Ag<sup>+</sup> releasing rate decreased gradually and finally reached a steady releasing rate of around 0.0018  $\mu\text{g cm}^{-2} \text{day}^{-1}$  from the 8<sup>th</sup> day. Such a low releasing rate could be attributed to the stability of CNC/Ag nanocomposites in membrane polyamide layer. With high surface to volume ratio, CNCs could serve as good carriers to stable Ag NPs and prevent rapid Ag leaching from CNC/Ag nanocomposites.<sup>26, 62</sup> In addition, CNC exhibited excellent compatibility in polymer matrix due to their large surface area,<sup>63</sup> which could also help with the stability of CNC/Ag in the polyamide layer. Besides the Ag releasing rate, the duration of antibacterial effectiveness is also a crucial factor in practical water treatment. The total Ag content in the CNC/Ag membrane (0.43  $\mu\text{g cm}^{-2}$ ) in this work is 36 times lower than the Ag NPs of membranes (15.5  $\mu\text{g cm}^{-2}$ ) synthesized in the study done by Yin et al.<sup>38</sup> (Table 2). However, the CNC/Ag TFN membrane was expected to be effective for around 222 days, which was much longer than

Yin et al.<sup>38</sup> (~ 140 days) and other reported Ag embedded membrane studies (97-155 days).<sup>45, 64, 65</sup> The Ag leaching results imply that CNC/Ag TFN membranes can achieve a low Ag releasing rate and longer duration time with a significant small amount of total Ag loading,

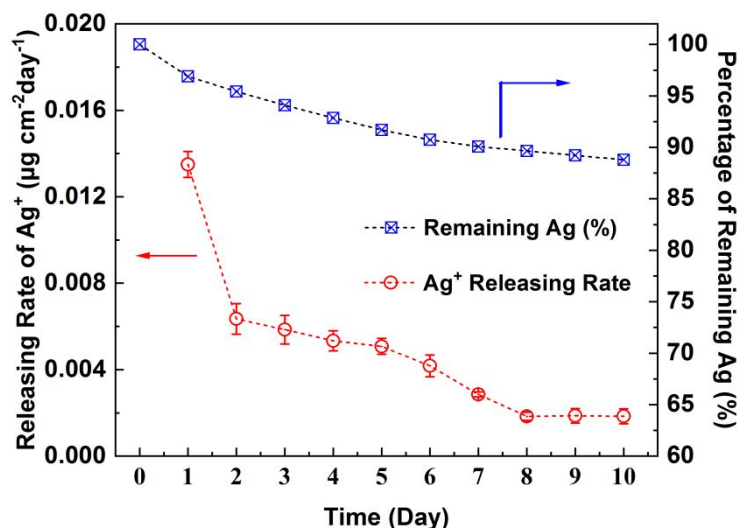


**Fig. 8** Ag<sup>+</sup> release profile of CNC/Ag-0.01 TFN membrane and its remaining percentage of Ag on membrane surface.

which implies its low potential environmental risks and the potential for practical water treatment.

#### 4. Conclusion

In this study, multifunctional thin film nanocomposites nanofiltration membranes were synthesized by embedding CNC/Ag nanocomposites into the thin active layer. A detailed benchmarking was presented in Table 2, which summarized the nanocomposite TFN membranes containing Ag NPs reported in recent years. Among all these membranes, the CNC/Ag-0.01 TFN NF membrane exhibited distinguishing multi-functions including high pure water flux, high salt rejection for Na<sub>2</sub>SO<sub>4</sub> (> 99 %), excellent antifouling and antibacterial performance simultaneously. CNC/Ag membranes with high flux and rejections

are more energy-efficient than TFC membranes, which reduces the energy consumption associated with the NF process. The excellent antifouling and antibacterial properties of the membrane can mitigate flux decline by preventing the formation of physical and biological fouling films, which improves the membrane durability in the long-term operation. Furthermore, the CNC/Ag-0.01 TFN NF membrane also demonstrated excellent Ag stability on the membrane surface, which not only enabled it to achieve high antibacterial performance at a very low Ag loading of  $0.43 \mu\text{g cm}^{-2}$  but also prevented the potential environmental hazard of excess Ag leaching. In addition, the relatively low cost and facile synthesis method of CNC/Ag nanocomposites will benefit the large-scale production of CNC/Ag TFN NF membranes. These results demonstrate that the multifunctional CNC/Ag TFN NF membranes may have a promising potential application in desalination and water treatment processes.

**Table 2.** Summary of recently reported nanocomposite TFN membranes containing Ag NPs and commercial NF membranes.

Membrane	Pure Water Permeability (LMH/bar)	Na <sub>2</sub> SO <sub>4</sub> Rejection (%)	Antibacterial performance for <i>E. coli</i> (%)	Total Ag loading ( $\mu\text{g cm}^{-2}$ )	Ref.
CNC/Ag-0.01 NF	25.4	99.1	99.4	0.4	This work
PEI/PEG/Ag NF	/	92	/	3.6	5
COO <sup>-</sup> zwitterion-Ag NF	/	~95	93.1	10.1	58
Ag-PDA-TFN NF	5.9	/	$55.6 \pm 13.7$	14.7	66
rGO/Ti <sub>2</sub> O/Ag NF	/	96%	> 90%	/	18
S-BioAg NF	5	85.5	/	/	67
S-ChemAg NF	5	87	/	2.3	67
CA/Ag NF	1.9	96.4	>99%	/	68
<i>In-situ</i> Ag RO	/	/	$78 \pm 12$	3.7	64
SH-AgNPs RO	4.4	/	/	15.5	38
NF 90	6.7	98.6	/	/	69

NF 270

11.2

94

/

/

70

## Conflicts of interest

There are no conflicts of interest to declare.

## Acknowledgements

This work is partially supported by U.S. Department of Agriculture (Grant No. 2018-68011-28371)

## References

1. C. Liu, A. F. Faria, J. Ma and M. Elimelech, Mitigation of biofilm development on thin-film composite membranes functionalized with zwitterionic polymers and silver nanoparticles, *Environmental science & technology*, 2016, **51**, 182-191.
2. Z. Wang, Z. Wang, S. Lin, H. Jin, S. Gao, Y. Zhu and J. Jin, Nanoparticle-templated nanofiltration membranes for ultrahigh performance desalination, *Nature communications*, 2018, **9**, 2004.
3. L. Bai, Y. Liu, N. Bossa, A. Ding, N. Ren, G. Li, H. Liang and M. R. Wiesner, Incorporation of Cellulose Nanocrystals (CNCs) into the Polyamide Layer of Thin-Film Composite (TFC) Nanofiltration Membranes for Enhanced Separation Performance and Antifouling Properties, *Environmental Science & Technology*, 2018, **52**, 11178-11187.
4. L. Bai, Y. Liu, A. Ding, N. Ren, G. Li and H. Liang, Fabrication and characterization of thin-film composite (TFC) nanofiltration membranes incorporated with cellulose nanocrystals (CNCs) for enhanced desalination performance and dye removal, *Chemical Engineering Journal*, 2019, **358**, 1519-1528.
5. A. Bera, J. S. Trivedi, S. B. Kumar, A. K. S. Chandel, S. Haldar and S. K. Jewrajka, Anti-organic fouling and anti-biofouling poly (piperazineamide) thin film nanocomposite membranes for low pressure removal of heavy metal ions, *Journal of hazardous materials*, 2018, **343**, 86-97.
6. H. B. Park, J. Kamcev, L. M. Robeson, M. Elimelech and B. D. Freeman, Maximizing the right stuff: The trade-off between membrane permeability and selectivity, *Science*, 2017, **356**, eaab0530.
7. J. H. Jhaveri and Z. Murthy, A comprehensive review on anti-fouling nanocomposite membranes for pressure driven membrane separation processes, *Desalination*, 2016, **379**, 137-154.
8. M. Elimelech and W. A. Phillip, The future of seawater desalination: energy, technology, and the environment, *science*, 2011, **333**, 712-717.
9. H. Shi, Y. He, Y. Pan, H. Di, G. Zeng, L. Zhang and C. Zhang, A modified mussel-inspired method to fabricate TiO<sub>2</sub> decorated superhydrophilic PVDF membrane for oil/water separation, *Journal of Membrane Science*, 2016, **506**, 60-70.
10. M. Obaid, Z. K. Ghouri, O. A. Fadali, K. A. Khalil, A. A. Almajid and N. A. M. Barakat, Amorphous SiO<sub>2</sub> NP-Incorporated Poly(vinylidene fluoride) Electrospun Nanofiber

- 1  
2  
3  
4  
5  
6  
7  
8  
9  
10  
11  
12  
13  
14  
15  
16  
17  
18  
19  
20  
21  
22  
23  
24  
25  
26  
27  
28  
29  
30  
31  
32  
33  
34  
35  
36  
37  
38  
39  
40  
41  
42  
43  
44  
45  
46  
47  
48  
49  
50  
51  
52  
53  
54  
55  
56  
57  
58  
59  
60
- Membrane for High Flux Forward Osmosis Desalination, *ACS Applied Materials & Interfaces*, 2016, **8**, 4561-4574.
11. M. Safarpour, A. Khataee and V. Vatanpour, Thin film nanocomposite reverse osmosis membrane modified by reduced graphene oxide/TiO<sub>2</sub> with improved desalination performance, *Journal of Membrane Science*, 2015, **489**, 43-54.
  12. P. F. Andrade, A. F. de Faria, S. R. Oliveira, M. A. Z. Arruda and M. d. C. Gonçalves, Improved antibacterial activity of nanofiltration polysulfone membranes modified with silver nanoparticles, *Water Research*, 2015, **81**, 333-342.
  13. J. Zhu, J. Wang, A. A. Uliana, M. Tian, Y. Zhang, Y. Zhang, A. Volodin, K. Simoens, S. Yuan, J. Li, J. Lin, K. Bernaerts and B. Van der Bruggen, Mussel-Inspired Architecture of High-Flux Loose Nanofiltration Membrane Functionalized with Antibacterial Reduced Graphene Oxide–Copper Nanocomposites, *ACS Applied Materials & Interfaces*, 2017, **9**, 28990-29001.
  14. Y. T. Chung, E. Mahmoudi, A. W. Mohammad, A. Benamor, D. Johnson and N. Hilal, Development of polysulfone-nanohybrid membranes using ZnO-GO composite for enhanced antifouling and antibacterial control, *Desalination*, 2017, **402**, 123-132.
  15. M. D. Firouzjaei, A. A. Shamsabadi, S. A. Aktij, S. F. Seyedpour, M. Sharifian Gh, A. Rahimpour, M. R. Esfahani, M. Ulbricht and M. Soroush, Exploiting synergetic effects of graphene oxide and a silver-based metal–organic framework to enhance antifouling and anti-biofouling properties of thin-film nanocomposite membranes, *ACS applied materials & interfaces*, 2018, **10**, 42967-42978.
  16. S.-Y. Kwak, S. H. Kim and S. S. Kim, Hybrid organic/inorganic reverse osmosis (RO) membrane for bactericidal anti-fouling. 1. Preparation and characterization of TiO<sub>2</sub> nanoparticle self-assembled aromatic polyamide thin-film-composite (TFC) membrane, *Environmental science & technology*, 2001, **35**, 2388-2394.
  17. Q. Zhang, S. Chen, X. Fan, H. Zhang, H. Yu and X. Quan, A multifunctional graphene-based nanofiltration membrane under photo-assistance for enhanced water treatment based on layer-by-layer sieving, *Applied Catalysis B: Environmental*, 2018, **224**, 204-213.
  18. H. Abadikhah, E. Naderi Kalali, S. Khodi, X. Xu and S. Agathopoulos, Multifunctional Thin Film Nanofiltration Membrane Incorporated with Reduced Graphene Oxide@ TiO<sub>2</sub>@ Ag Nanocomposites for High Desalination Performance, Dye Retention, and Antibacterial Properties, *ACS applied materials & interfaces*, 2019.
  19. H. M. Hegab, A. ElMekawy, T. G. Barclay, A. Michelmore, L. Zou, C. P. Saint and M. Ginic-Markovic, Single-step assembly of multifunctional poly (tannic acid)–graphene oxide coating to reduce biofouling of forward osmosis membranes, *ACS applied materials & interfaces*, 2016, **8**, 17519-17528.
  20. C. Marambio-Jones and E. M. Hoek, A review of the antibacterial effects of silver nanomaterials and potential implications for human health and the environment, *Journal of Nanoparticle Research*, 2010, **12**, 1531-1551.
  21. G. Jia, H. Wang, L. Yan, X. Wang, R. Pei, T. Yan, Y. Zhao and X. Guo, Cytotoxicity of carbon nanomaterials: single-wall nanotube, multi-wall nanotube, and fullerene, *Environmental science & technology*, 2005, **39**, 1378-1383.
  22. O. Akhavan and E. Ghaderi, Toxicity of graphene and graphene oxide nanowalls against bacteria, *ACS nano*, 2010, **4**, 5731-5736.

- 1
- 2
- 3
- 4 23. D. Klemm, F. Kramer, S. Moritz, T. Lindström, M. Ankerfors, D. Gray and A. Dorris,  
5 Nanocelluloses: a new family of nature-based materials, *Angewandte Chemie International*  
6 *Edition*, 2011, **50**, 5438-5466.
- 7
- 8 24. N. Mohammed, N. Grishkewich and K. C. Tam, Cellulose nanomaterials: Promising  
9 sustainable nanomaterials for application in water/wastewater treatment processes,  
10 *Environmental Science: Nano*, 2018, **5**, 623-658.
- 11
- 12 25. L. Bai, N. Bossa, F. Qu, J. Winglee, G. Li, K. Sun, H. Liang and M. R. Wiesner, Comparison of  
13 hydrophilicity and mechanical properties of nanocomposite membranes with cellulose  
14 nanocrystals and carbon nanotubes, *Environmental science & technology*, 2016, **51**, 253-262.
- 15
- 16 26. A. W. Carpenter, C.-F. de Lannoy and M. R. Wiesner, Cellulose nanomaterials in water  
17 treatment technologies, *Environmental science & technology*, 2015, **49**, 5277-5287.
- 18
- 19 27. O. Choi, K. K. Deng, N.-J. Kim, L. Ross Jr, R. Y. Surampalli and Z. Hu, The inhibitory effects of  
20 silver nanoparticles, silver ions, and silver chloride colloids on microbial growth, *Water*  
21 *research*, 2008, **42**, 3066-3074.
- 22
- 23 28. M. S. Mauter, Y. Wang, K. C. Okemgbo, C. O. Osuji, E. P. Giannelis and M. Elimelech,  
24 Antifouling ultrafiltration membranes via post-fabrication grafting of biocidal nanomaterials,  
25 *ACS applied materials & interfaces*, 2011, **3**, 2861-2868.
- 26
- 27 29. F. Mafuné, J.-y. Kohno, Y. Takeda, T. Kondow and H. Sawabe, Structure and stability of silver  
28 nanoparticles in aqueous solution produced by laser ablation, *The Journal of Physical*  
29 *Chemistry B*, 2000, **104**, 8333-8337.
- 30
- 31 30. H. Liu, J. Song, S. Shang, Z. Song and D. Wang, Cellulose Nanocrystal/Silver Nanoparticle  
32 Composites as Bifunctional Nanofillers within Waterborne Polyurethane, *ACS Applied*  
33 *Materials & Interfaces*, 2012, **4**, 2413-2419.
- 34
- 35 31. F. Fu, J. Gu, J. Cao, R. Shen, H. Liu, Y. Zhang, X. Liu and J. Zhou, Reduction of silver ions using  
36 an alkaline cellulose dope: straightforward access to Ag/ZnO decorated cellulose  
37 nanocomposite film with enhanced antibacterial activities, *ACS Sustainable Chemistry &*  
38 *Engineering*, 2017, **6**, 738-748.
- 39
- 40 32. F. Rashidi, N. S. Kevlich, S. A. Sinquefield, M. L. Shofner and S. Nair, Graphene oxide  
41 membranes in extreme operating environments: concentration of kraft black liquor by lignin  
42 retention, *ACS Sustainable Chemistry & Engineering*, 2016, **5**, 1002-1009.
- 43
- 44 33. Z. Wang, C. Ma, S. A. Sinquefield, M. L. Shofner and S. Nair, High-Performance Graphene  
45 Oxide Nanofiltration Membranes for Black Liquor Concentration, *ACS Sustainable Chemistry*  
46 *& Engineering*, 2019, **7**, 14915-14923.
- 47
- 48 34. Y. Han, Y. Jiang and C. Gao, High-flux graphene oxide nanofiltration membrane intercalated  
49 by carbon nanotubes, *ACS applied materials & interfaces*, 2015, **7**, 8147-8155.
- 50
- 51 35. M. Wu, T. Ma, Y. Su, H. Wu, X. You, Z. Jiang and R. Kasher, Fabrication of composite  
52 nanofiltration membrane by incorporating attapulgite nanorods during interfacial  
53 polymerization for high water flux and antifouling property, *Journal of Membrane Science*,  
54 2017, **544**, 79-87.
- 55
- 56 36. W. Chen, J. Jiang, W. Zhang, T. Wang, J. Zhou, C.-H. Huang and X. Xie, Silver  
57 Nanowire-Modified Filter with Controllable Silver Ion Release for Point-of-Use Disinfection,  
58 *Environmental science & technology*, 2019, **53**, 7504-7512.
- 59
- 60

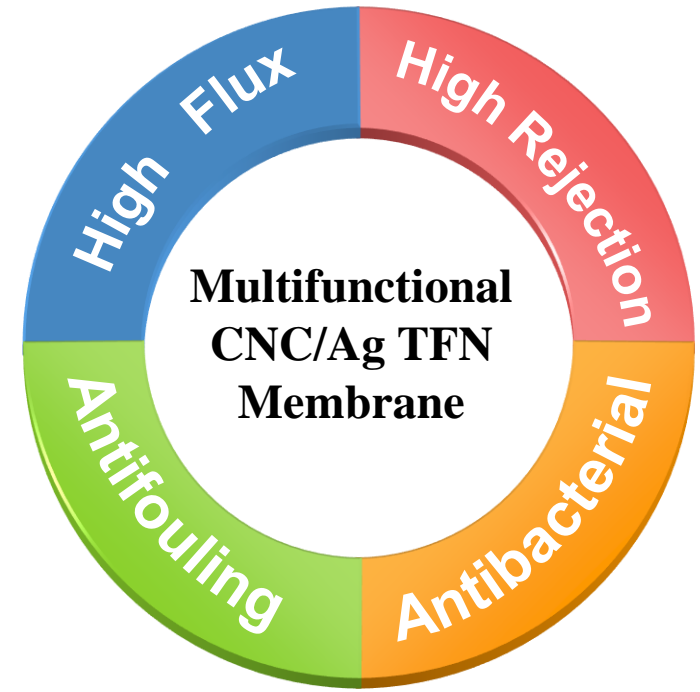
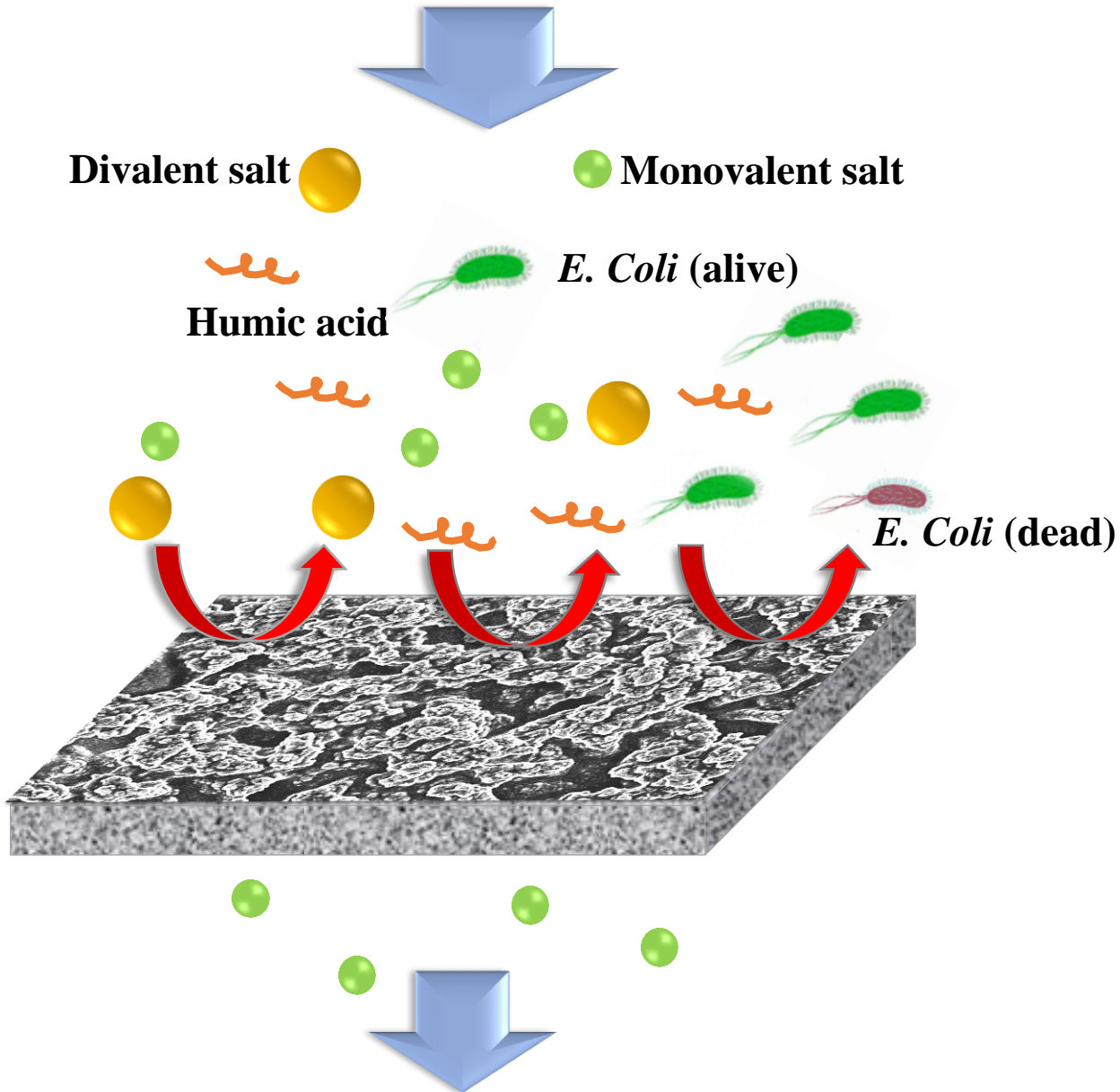
- 1  
2  
3  
4 37. F. Perreault, M. E. Tousley and M. Elimelech, Thin-Film Composite Polyamide Membranes  
5 Functionalized with Biocidal Graphene Oxide Nanosheets, *Environmental Science &*  
6 *Technology Letters*, 2014, **1**, 71-76.
- 7 38. J. Yin, Y. Yang, Z. Hu and B. Deng, Attachment of silver nanoparticles (AgNPs) onto thin-film  
8 composite (TFC) membranes through covalent bonding to reduce membrane biofouling,  
9 *Journal of membrane science*, 2013, **441**, 73-82.
- 10 39. D. Koushik, S. Sen Gupta, S. M. Maliyekkal and T. Pradeep, Rapid dehalogenation of  
11 pesticides and organics at the interface of reduced graphene oxide–silver nanocomposite,  
12 *Journal of Hazardous Materials*, 2016, **308**, 192-198.
- 13 40. A. F. Faria, C. Liu, M. Xie, F. Perreault, L. D. Nghiem, J. Ma and M. Elimelech, Thin-film  
14 composite forward osmosis membranes functionalized with graphene oxide–silver  
15 nanocomposites for biofouling control, *Journal of Membrane Science*, 2017, **525**, 146-156.
- 16 41. X. You, T. Ma, Y. Su, H. Wu, M. Wu, H. Cai, G. Sun and Z. Jiang, Enhancing the permeation  
17 flux and antifouling performance of polyamide nanofiltration membrane by incorporation of  
18 PEG-POSS nanoparticles, *Journal of Membrane Science*, 2017, **540**, 454-463.
- 19 42. X. Zhang, Y. Lv, H.-C. Yang, Y. Du and Z.-K. Xu, Polyphenol coating as an interlayer for  
20 thin-film composite membranes with enhanced nanofiltration performance, *ACS applied*  
21 *materials & interfaces*, 2016, **8**, 32512-32519.
- 22 43. X. Zhu, H. Liang, X. Tang, L. Bai, X. Zhang, Z. Gan, X. Cheng, X. Luo, D. Xu and G. Li,  
23 Supramolecular-based Regenerable Coating Layer of Thin-Film Composite Nanofiltration  
24 Membrane for Simultaneously Enhanced Desalination and Antifouling Properties, *ACS*  
25 *applied materials & interfaces*, 2019.
- 26 44. F. Asempour, D. Emadzadeh, T. Matsuura and B. Kruczek, Synthesis and characterization of  
27 novel Cellulose Nanocrystals-based Thin Film Nanocomposite membranes for reverse  
28 osmosis applications, *Desalination*, 2018, **439**, 179-187.
- 29 45. S.-H. Park, S. H. Kim, S.-J. Park, S. Ryoo, K. Woo, J. S. Lee, T.-S. Kim, H.-D. Park, H. Park and  
30 Y.-I. Park, Direct incorporation of silver nanoparticles onto thin-film composite membranes  
31 via arc plasma deposition for enhanced antibacterial and permeation performance, *Journal*  
32 *of membrane science*, 2016, **513**, 226-235.
- 33 46. Z. Liu, L. Qi, X. An, C. Liu and Y. Hu, Surface engineering of thin film composite polyamide  
34 membranes with silver nanoparticles through layer-by-layer interfacial polymerization for  
35 antibacterial properties, *ACS applied materials & interfaces*, 2017, **9**, 40987-40997.
- 36 47. Z. Tan, S. Chen, X. Peng, L. Zhang and C. Gao, Polyamide membranes with nanoscale Turing  
37 structures for water purification, *Science*, 2018, **360**, 518-521.
- 38 48. P. Qu, H. Tang, Y. Gao, L. Zhang and S. Wang, Polyethersulfone composite membrane  
39 blended with cellulose fibrils, *BioResources*, 2010, **5**, 2323-2336.
- 40 49. R. Zhang, S. Yu, W. Shi, W. Wang, X. Wang, Z. Zhang, L. Li, B. Zhang and X. Bao, A novel  
41 polyesteramide thin film composite nanofiltration membrane prepared by interfacial  
42 polymerization of serinol and trimesoyl chloride (TMC) catalyzed by  
43 4-dimethylaminopyridine (DMAP), *Journal of Membrane Science*, 2017, **542**, 68-80.
- 44 50. D. Y. Koseoglu-Imer, B. Kose, M. Altinbas and I. Koyuncu, The production of polysulfone (PS)  
45 membrane with silver nanoparticles (AgNP): physical properties, filtration performances,  
46 and biofouling resistances of membranes, *Journal of membrane science*, 2013, **428**, 620-628.
- 47  
48  
49  
50  
51  
52  
53  
54  
55  
56  
57  
58  
59  
60

- 1  
2  
3  
4 51. A. F. De Faria, F. o. Perreault, E. Shaulsky, L. H. Arias Chavez and M. Elimelech, Antimicrobial  
5 electrospun biopolymer nanofiber mats functionalized with graphene oxide–silver  
6 nanocomposites, *ACS applied materials & interfaces*, 2015, **7**, 12751-12759.
- 7 52. L.-x. Dong, X.-c. Huang, Z. Wang, Z. Yang, X.-m. Wang and C. Y. Tang, A thin-film  
8 nanocomposite nanofiltration membrane prepared on a support with in situ embedded  
9 zeolite nanoparticles, *Separation and Purification Technology*, 2016, **166**, 230-239.
- 10 53. R. N. Wenzel, Resistance of solid surfaces to wetting by water, *Industrial & Engineering  
11 Chemistry*, 1936, **28**, 988-994.
- 12 54. G.-d. Kang and Y.-m. Cao, Development of antifouling reverse osmosis membranes for water  
13 treatment: a review, *Water research*, 2012, **46**, 584-600.
- 14 55. X. Hao, S. Gao, J. Tian, Y. Sun, F. Cui and C. Y. Tang, Calcium-Carboxyl Intrabridging during  
15 Interfacial Polymerization: A Novel Strategy to Improve Antifouling Performance of Thin Film  
16 Composite Membranes, *Environmental science & technology*, 2019, **53**, 4371-4379.
- 17 56. J. Yin and B. Deng, Polymer-matrix nanocomposite membranes for water treatment, *Journal  
18 of membrane science*, 2015, **479**, 256-275.
- 19 57. J. Lv, G. Zhang, H. Zhang, C. Zhao and F. Yang, Improvement of antifouling performances for  
20 modified PVDF ultrafiltration membrane with hydrophilic cellulose nanocrystal, *Applied  
21 Surface Science*, 2018, **440**, 1091-1100.
- 22 58. M. Yi, C. H. Lau, S. Xiong, W.-J. Wei, R.-Z. Liao, L. Shen, A. Lu and Y. Wang, Zwitterion-Ag  
23 complexes that simultaneously enhance biofouling resistance and silver binding capability of  
24 thin film composite membranes, *ACS applied materials & interfaces*, 2019.
- 25 59. A. Zirehpour, A. Rahimpour, A. Arabi Shamsabadi, M. Sharifian Gh and M. Soroush,  
26 Mitigation of thin-film composite membrane biofouling via immobilizing nano-sized biocidal  
27 reservoirs in the membrane active layer, *Environmental science & technology*, 2017, **51**,  
28 5511-5522.
- 29 60. E.-S. Kim, G. Hwang, M. G. El-Din and Y. Liu, Development of nanosilver and multi-walled  
30 carbon nanotubes thin-film nanocomposite membrane for enhanced water treatment,  
31 *Journal of membrane science*, 2012, **394**, 37-48.
- 32 61. J. Li, L. Kang, B. Wang, K. Chen, X. Tian, Z. Ge, J. Zeng, J. Xu and W. Gao, Controlled Release  
33 and Long-Term Antibacterial Activity of Dialdehyde Nanofibrillated Cellulose/Silver  
34 Nanoparticle Composites, *ACS Sustainable Chemistry & Engineering*, 2018, **7**, 1146-1158.
- 35 62. A. Sheikhi, S. Safari, H. Yang and T. G. van de Ven, Copper removal using electrosterically  
36 stabilized nanocrystalline cellulose, *ACS applied materials & interfaces*, 2015, **7**,  
37 11301-11308.
- 38 63. X. Xu, Y.-Q. Yang, Y.-Y. Xing, J.-F. Yang and S.-F. Wang, Properties of novel polyvinyl  
39 alcohol/cellulose nanocrystals/silver nanoparticles blend membranes, *Carbohydrate  
40 polymers*, 2013, **98**, 1573-1577.
- 41 64. M. Ben-Sasson, X. Lu, E. Bar-Zeev, K. R. Zodrow, S. Nejati, G. Qi, E. P. Giannelis and M.  
42 Elimelech, In situ formation of silver nanoparticles on thin-film composite reverse osmosis  
43 membranes for biofouling mitigation, *Water research*, 2014, **62**, 260-270.
- 44 65. S.-H. Park, Y.-S. Ko, S.-J. Park, J. S. Lee, J. Cho, K.-Y. Baek, I. T. Kim, K. Woo and J.-H. Lee,  
45 Immobilization of silver nanoparticle-decorated silica particles on polyamide thin film  
46 composite membranes for antibacterial properties, *Journal of Membrane Science*, 2016, **499**,  
47 80-91.
- 48  
49  
50  
51  
52  
53  
54  
55  
56  
57  
58  
59  
60

- 1  
2  
3  
4  
5  
6  
7  
8  
9  
10  
11  
12  
13  
14  
15  
16  
17  
18  
19  
20  
21  
22  
23  
24  
25  
26  
27  
28  
29  
30  
31  
32  
33  
34  
35  
36  
37  
38  
39  
40  
41  
42  
43  
44  
45  
46  
47  
48  
49  
50  
51  
52  
53  
54  
55  
56  
57  
58  
59  
60
66. Z. Yang, Y. Wu, H. Guo, X.-H. Ma, C.-E. Lin, Y. Zhou, B. Cao, B.-K. Zhu, K. Shih and C. Y. Tang, A novel thin-film nano-templated composite membrane with in situ silver nanoparticles loading: Separation performance enhancement and implications, *Journal of Membrane Science*, 2017, **544**, 351-358.
67. S. Liu, F. Fang, J. Wu and K. Zhang, The anti-biofouling properties of thin-film composite nanofiltration membranes grafted with biogenic silver nanoparticles, *Desalination*, 2015, **375**, 121-128.
68. S. Beisl, S. Monteiro, R. Santos, A. S. Figueiredo, M. G. Sánchez-Loredo, M. A. Lemos, F. Lemos, M. Minhalma and M. N. De Pinho, Synthesis and bactericide activity of nanofiltration composite membranes—Cellulose acetate/silver nanoparticles and cellulose acetate/silver ion exchanged zeolites, *Water research*, 2019, **149**, 225-231.
69. C. Liu, L. Shi and R. Wang, Crosslinked layer-by-layer polyelectrolyte nanofiltration hollow fiber membrane for low-pressure water softening with the presence of SO<sub>4</sub><sup>2-</sup> in feed water, *Journal of Membrane Science*, 2015, **486**, 169-176.
70. J. Miao, R. Zhang and R. Bai, Poly (vinyl alcohol)/carboxymethyl cellulose sodium blend composite nanofiltration membranes developed via interfacial polymerization, *Journal of Membrane Science*, 2015, **493**, 654-663.

# Table of Content

- Multifunctional CNC/Ag thin film nanocomposite nanofiltration membranes with high flux, high rejection, excellent antifouling and antibacterial performance.



- Pure water permeance: 25.44 LMH/bar
- $\text{Na}_2\text{SO}_4$  rejection > 99%
- Flux recovery ratio > 90 %
- *E coli*. Inhibition > 99%